JOURNAL OF CATALYSIS 138, 150–163 (1992)

Characterization of Dealuminated Large-Port Mordenites

MILES J. VAN NIEKERK, JACK C. Q. FLETCHER, AND CYRIL T. O'CONNOR

Catalysis Research Unit, Department of Chemical Engineering, University of Cape Town, Rondebosch, 7700, Republic of South Africa

Received October 9, 1991; revised April 21, 1992

Four different types of large-port mordenite were studied. Three of these catalyst samples were dealuminated by treatment with nitric acid and were characterized by temperature-programmed desorption (TPD) of ammonia, infrared spectroscopy, cyclohexane adsorption, solid-state NMR, and X-ray diffraction (XRD). It was found that the extent of dealumination and the amount of octahedral aluminum remaining in the zeolite channels was strongly influenced by crystallite size. Extensive dealumination resulted in materials with surface areas greater than the parent materials, yet still retaining their characteristic mordenite structure as determined by XRD. Ammonia TPD was shown to uniquely determine the framework aluminum content, irrespective of the presence of extraframework aluminum. The previously disputed origin of the infrared absorption band at 955 cm^{-1} is assigned to new Si–O–Si bonds formed upon framework dealumination. A sequence of dealumination events is proposed.

INTRODUCTION

It has been reported that dealuminated mordenites show improved lifetimes for a number of chemical reactions (*1–10*). Mordenite may be synthesized with Si/Al ratios ranging between 4.5 and 10 (*11*) and further dealumination is often accomplished by acid leaching, steam treatment, or heat treatments, which may result in a transformation of small-port mordenite into large-port mordenite (*12–14*).

Much of the attention of workers studying the dealumination of mordenite by acid treatment has been focused on the modification of small-port mordenite. In the present investigation, a number of characterization techniques have been used to study the dealumination process of large-port mordenite. The influence of crystallite size on the extent of dealumination and on the residual octahedral aluminum content is reported.

A number of assignments have been proposed for the structural infrared bands in the two regions 930–960 and 620–630 cm^{-1}. The band between 930 and 960 cm^{-1}, sometimes seen in dealuminated samples, has been assigned to hydroxyl nests by Beyer *et al.* (*15*) and to the formation of new Si–O bonds by others (*16–18*). The 620–630 cm^{-1} band has been assigned to vibrations in single 4-rings (*19*), alternating SiO_4 and AlO_4 tetrahedra (*20*), and, more recently, to isolated AlO_4 tetrahedra in single 4-rings (*13*). The results of this study provide clear support for some of the above-mentioned assignments. This paper presents the results of an investigation into the effect of dealumination, via acid washing, on the properties of three different large-port mordenite materials and also the properties of a range of commercially available dealuminated mordenites.

EXPERIMENTAL

Catalysts

The catalysts used in the study were Zeocat mordenite (ZM), Norton mordenite Z900 (NM), and mordenite synthesized according to the method of Itabashi *et al.* (*11*). Samples with three different aluminum contents were obtained from Zeocat and are referred to as ZM510, ZM760, and ZM980. These samples were dealuminated by steam treatment followed by acid treatment. The Norton mor-

0021-9517/92 $5.00

denite was obtained as $\frac{1}{16}$-in. binderless extrudates in the sodium form. In the manufacture of the extrudates it is possible that a viscosity modifier such as hydroxymethylcellulose was used. This would, however, be removed by combustion during the calcination process. This material was crushed and sieved and particles of less than 75 μm were used in this study. No indication of the presence of any foreign material was found in the ZM and NM samples by either XRD or electron microscopy. Two batches of mordenite were synthesized in a mechanically stirred autoclave at 190°C under autothermal pressure. The first batch was synthesized at an autoclave impeller speed of 300 rpm (S1) and the second at an impeller speed of 30 rpm (S2). The molar ratio of both synthesis mixtures was $Na_2O/Al_2O_3/SiO_2/H_2O$: 1.7/1/11.5/230, and the synthesis time was 48 h. The sodium and hydrogen forms of all the above catalysts are designated -Na and -H, respectively. Hydrogen form samples were obtained by calcination of the ammonium forms in air at 400°C for 8 h.

Dealumination Procedure

The dealumination procedure used was that described by Karge *et al.* (*21*). Samples designated -1 *N* and -6 *N* were prepared by stirring 1.0 g of sodium mordenite in 27 ml of 1 *N* and 6 *N* HNO_3 respectively, at room temperature. These samples were then washed in 1 liter of flowing distilled water, dried overnight at 90°C, and crushed to less than 75 μm particle size. Samples designated -01 were prepared by stirring 4 g of sodium mordenite in 53 ml of 6 *N* HNO_3 for 4 h at room temperature, washing, drying, and crushing and repeating these treatments once. More severely dealuminated samples were prepared by multiple cycles of refluxing 4 g of sodium mordenite in 53 ml of 6 *N* HNO_3 for 4 h and then washing, drying, and crushing as described above. Samples undergoing two and four such refluxing cycles are designated -02 and -03, respectively. The S1 samples S1-02 II and S1-03 II were prepared according to the same procedures as the S1-02 and S1-03 samples but the ammonium form of the catalyst was used in place of the sodium form. These samples are indicated by the suffix II.

Catalyst Characterization

Catalyst aluminum contents were determined by atomic absorption (AA). For this purpose, samples were prepared by dissolving 100 mg of the catalyst in hydrofluoric/hydrochloric acid (5 ml 40% HF, 5 ml 31% HCl) at room temperature. After dissolution, 20 ml of a saturated boric acid solution was added to complex the excess hydrofluoric acid and the resulting solution made up to 50 ml using distilled water. AA standards were prepared using hydrofluoric, hydrochloric, and boric acid concentrations corresponding to those used for sample preparation.

^{27}Al MAS NMR spectra were recorded using a Bruker AM 300 spectrometer at a spin rate of 5000 Hz, a pulse width of 1.5 μs, a pulse angle of 30°, a relaxation delay of 0.1 s and employing $AlCl_3(H_2O)_6$ as an external standard at 0 ppm. Prior to NMR analysis, samples were calcined in air at 400°C for 8 h and allowed to equilibrate under ambient conditions. Catalyst agglomerate sizes were measured using a Malvern 2600/3600 particle sizer. Ammonia temperature-programmed desorption (NH_3 TPD) spectra were recorded in the range 100 to 650°C (0.5-g sample, 10°C/min temperature ramp, 60 ml/min helium carrier). Ammonia was preadsorbed at 100°C and TPD peak temperatures were reproducible to within 5°C. All the TPD spectra displayed two characteristic desorption peaks and for integration purposes these peaks were separated by dropping a perpendicular line from the trough between the two peaks to the baseline of the spectra.

X-ray diffraction (XRD) spectra were obtained using Cu$K\alpha$ radiation. The lattice constants *a*, *b*, and *c* were measured from the (200), (020), and (004) reflections, respectively. The relative crystallinities of the

zeolite samples were estimated by summing the peak heights of the (200), (111), (310), (202), (350), and (402) reflections and normalizing to 100% with respect to ZM980. For all catalysts, relative crystallinity data were obtained under identical instrumental and sample conditions. Surface areas were measured by nitrogen adsorption using standard BET apparatus after sample evacuation at 250°C. All samples used for BET and XRD analyses had been precalcined in air at 400°C for 8 h and allowed to cool at ambient conditions overnight.

Infrared spectra were recorded using a Nicolet 5ZDX FTIR spectrometer and are presented as transmittance spectra. The catalyst samples were calcined at 400°C and diluted 1 : 100 in KBr for viewing the 400–900 cm^{-1} bands and 1 : 500 for viewing the 1050–1090 cm^{-1} bands. Cyclohexane adsorption levels were determined at 70°C using a Stanton Redcroft STA 780 thermogravimetric balance. The cyclohexane partial pressure was 125-mm Hg.

RESULTS

Structure and Morphology

X-ray diffraction patterns of all the samples showed that the catalyst samples maintained the mordenite crystal structure throughout all the acid treatments. The unit cell volumes listed in Table 1 were calculated from the lattice constants *a*, *b*, and *c*. Generally, the unit cell volumes of NM, S1, and S2 decreased on dealumination. The unit cell volumes of the ZM samples were essentially the same. The length of the *c* axis did not vary significantly between catalyst samples, the most significant changes taking place in the direction of the *b* axis.

The relative crystallinities of the S2 samples were noticeably lower than those of the other samples (Table 1). The ZM samples had the highest percentage crystallinities, with the percentage crystallinities of the NM, S1, and S2 samples generally decreasing with decreasing aluminum content, whereas those of the ZM samples increased.

Electron microscopy showed that the catalyst crystallite sizes and morphologies varied considerably from one catalyst to another (Figure 1). The NM samples consisted of 10- to 30-μm intergrown crystals. The ZM samples consisted of 10- to 50-μm agglomerates of 1- to 5-μm crystals, some of which are intergrown. The S1 samples consisted of 3- to 10-μm agglomerates of 0.1–0.5 μm crystals which were uniform in size and shape.

The S2 mordenite consisted of two different types of agglomerates, both of which were made up of long needle-shaped crystals. The first agglomerate type consisted of tightly packed bundles of crystals about 1 μm long and 0.1 μm in diameter. The second agglomerate type, which made up most of the material, consisted of randomly orientated crystals which are about twice the size of those in the agglomerates of the first type. None of the morphologies, as described above, were observed to change, even after severe dealumination.

Catalyst Dealumination

The sodium forms of the NM, S1, and S2 samples had approximately the same aluminum content. Only trace quantities of sodium were found in the -01, -02, and -03 forms of these samples, whereas the -1 *N* and -6 *N* samples contained between 0.5 and 1% sodium. After undergoing identical dealumination procedures it was found that the NM, S1, and S2 mordenite materials retained vastly different aluminum contents (Table 2). In the case of the S1 mordenite, the aluminum content was reduced by 85% during the first refluxing procedure (S1–02) and further refluxing reduced the aluminum content by only an additional 1% of the original amount. In contrast, the NM and S2 materials retained much higher aluminum levels even after four acid refluxing cycles. From these results it is apparent that dealumination may reach a limit after removal of approximately seven-eighths of the initial aluminum content. Removal of the remaining one-eighth of the aluminum, corresponding to approximately one aluminum

TABLE 1

Characterization Data: Infrared T-0 Band Positions, Cyclohexane Adsorption Levels, Unit Cell Parameters, Relative Crystallinities, and Surface Areas

Catalyst	Tetrahedral aluminum (wt%)	Infrared T-0 band (1/cm)	Cyclohexane adsorbed (wt%)	Unit cell parameters (Å)			Unit cell volume (Å^3)	Relative crystallinity (%)	Surface area (m^2/g)
				a	*b*	*c*			
NM-Na	6.09	1044	8.8	18.18	20.54	7.52	2805	92	—
NM-H	6.19	1069	7.6	18.22	20.40	7.50	2788	89	396
NM-1 *N*	5.95	1074	8.5	18.14	20.53	7.50	2792	87	—
NM-6 *N*	5.52	1075	9.1	18.19	20.47	7.49	2789	94	—
NM-01	4.19	1080	7.6	18.20	20.35	7.50	2778	87	369
NM-02	3.02	1081	7.1	18.16	20.26	7.48	2752	85	373
NM-03	2.30	1083	6.7	18.14	20.23	7.47	2741	80	489
ZM510	3.17	1081	6.4	18.18	20.38	7.47	2768	82	410
ZM760	0.77	1087	6.2	18.18	20.40	7.48	2774	97	496
ZM980	0.43	1089	5.6	18.18	20.38	7.48	2771	100	490
S1-Na	6.50	1045	9.3	18.18	20.59	7.54	2822	85	—
S1-H	6.53	1060	9.1	18.24	20.37	7.51	2790	76	450
S1-1 *N*	5.88	1058	9.7	18.23	20.45	7.50	2796	76	—
S1-6 *N*	5.44	1062	10.2	18.26	20.49	7.50	2806	71	—
S1-01	3.89	1060	9.2	18.22	20.35	7.51	2785	71	375
S1-02	0.85	—	4.9	18.09	20.12	7.42	2701	64	447
S1-03	0.85	—	4.1	18.10	20.21	7.44	2722	73	486
S1-02II	0.89	1086	5.0	18.05	20.03	7.41	2679	66	453
S1-03II	0.86	1086	3.5	18.07	20.17	7.43	2708	73	450
S2-Na	6.41	1045	7.0	18.20	20.59	7.53	2822	75	—
S2-H	5.68	1073	6.8	18.17	20.33	7.49	2767	61	—
S2-1 *N*	5.42	1074	7.5	18.20	20.52	7.50	2801	69	—
S2-6 *N*	5.21	1075	7.7	18.20	20.52	7.50	2801	73	—
S2-01	4.78	1077	7.3	18.14	20.28	7.49	2755	59	—
S2-02	3.21	1083	6.6	18.15	20.26	7.48	2790	51	354
S2-03	2.33	1084	6.2	18.12	20.28	7.46	2741	58	378

per unit cell, may require more severe dealumination conditions. It is apparent from the characterization data of the S1-02/-03 and the Si-02 II/-03 II samples that the type of cation present (Na^+ or NH_4^+) in the mordenite samples did not affect the dealumination characteristics of these samples.

The framework aluminum is generally taken as the tetrahedral aluminum as determined by ^{27}Al MAS NMR (*13, 14, 22*), the results of which are shown in Table 2. Fernandez *et al.* (*23*) found that the ratio of (octahedral aluminum)/(tetrahedral aluminum) ^{27}Al NMR peak intensities increased as the pulse angle was increased and proposed that the relative concentrations of these species should be determined at very low pulse angles. However, for pulse angles up to 30°, the reported variation in the (tetrahedral aluminum)/(total aluminum) ratio for dealuminated mordenite is less than 10% (*23*). Due to the low aluminum content of the severely dealuminated samples, a pulse angle of 30° was required in this study to obtain adequate signal intensities. For the above reason, the tetrahedral aluminum contents reported in Tables 1 and 2 are subject to an error margin of approximately 10%.

NM-H contained 98% tetrahedral aluminum, this value dropping on initial acid refluxing to 62% and then increasing slightly

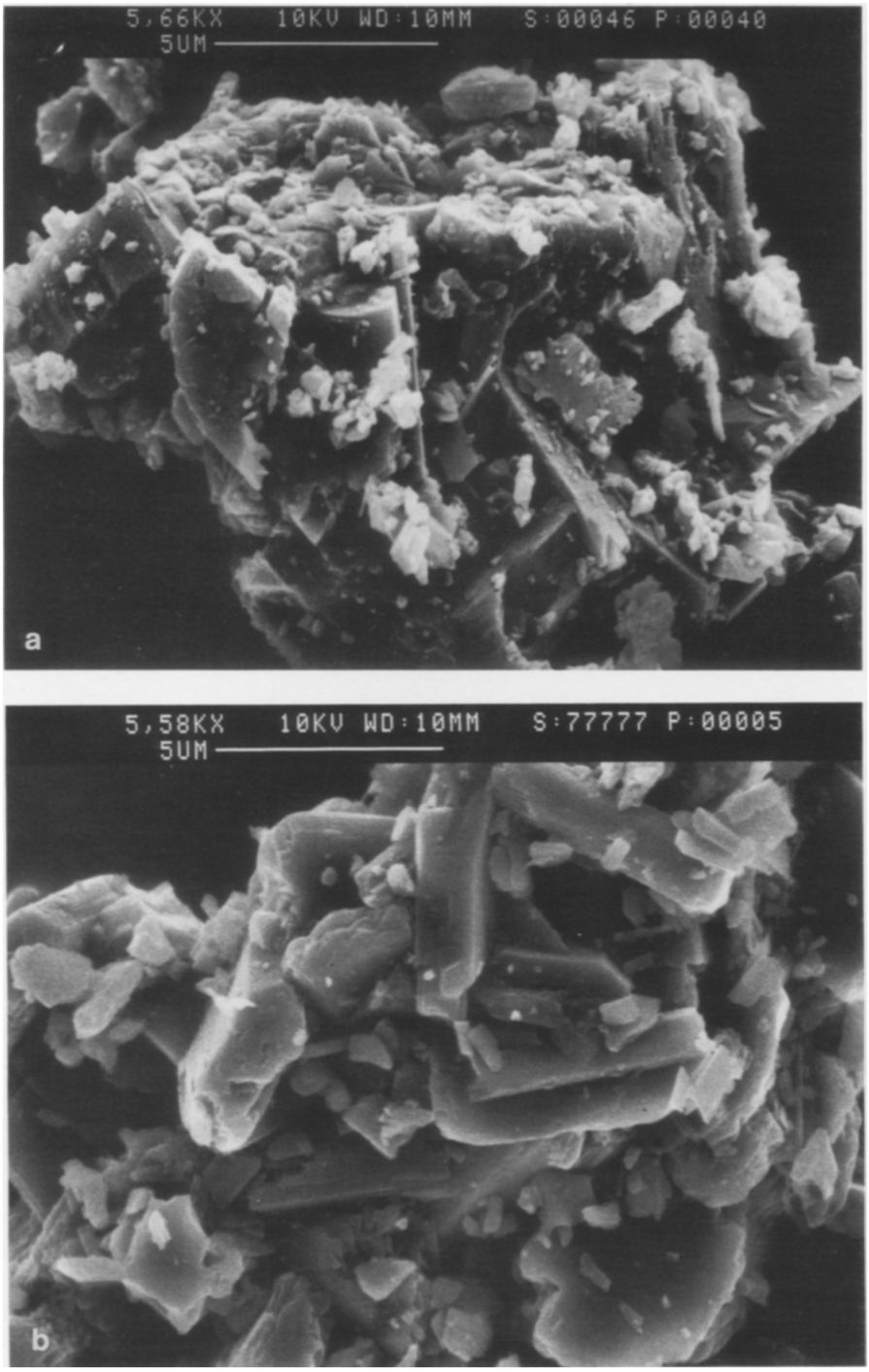

FIG. 1. Electron micrographs of dealuminated mordenites; (a) NM mordenite, (b) ZM mordenite, (c) S1 mordenite, (d) S2 mordenite.

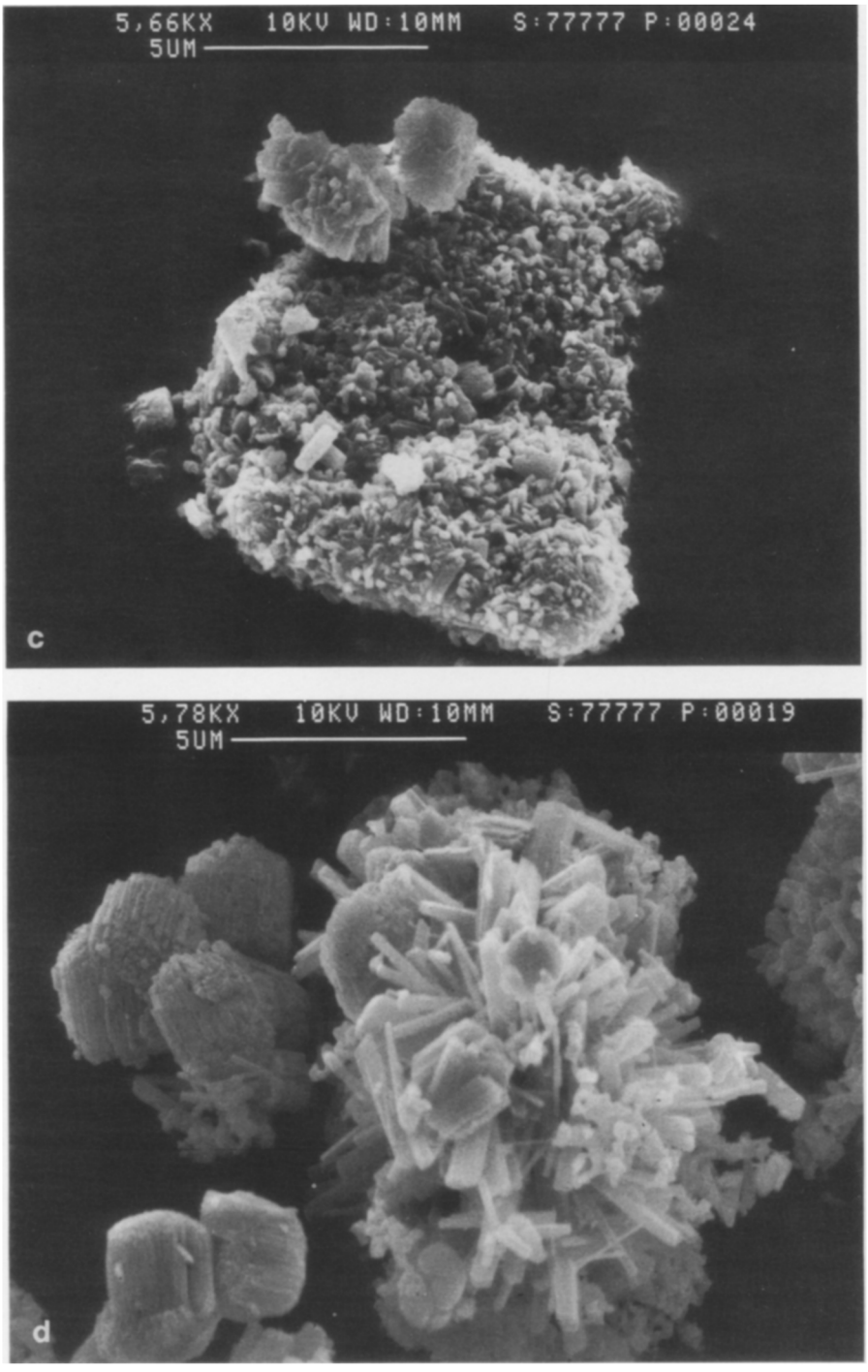

FIG. 1—*Continued*

TABLE 2

Characterization Data: ^{27}Al MAS NMR Tetrahedral Aluminum Peak Widths, Catalyst Water Content, and NH_3 TPD Peak Maxima and Concentrations (HTD/LTD: High-Temperature Desorption/Low-Temperature Desorption Peaks)

Catalyst	Total aluminum (wt%)	Tetrahedral aluminum (wt%)	^{27}Al NMR Al^{VI} width (ppm)	Water content (g/g dry cat.)	LTD TPD peak		HTD TPD peak	
					Temperature (°C)	NH_3 desorbed (mmol/g cat.)	Temperature (°C)	NH_3 desorbed (mmol/g cat.)
NM-Na	6.17	6.09	16.0	0.123	—	—	—	—
NM-H	6.34	6.19	12.8	0.109	229	0.91	615	1.77
NM-1 *N*	6.32	5.95	25.4	0.124	231	0.94	590	1.73
NM-6 *N*	6.03	5.52	23.9	0.125	225	0.94	598	1.92
NM-01	5.82	4.19	14.8	0.152	244	1.05	601	1.65
NM-02	4.88	3.02	5.1	0.140	237	0.80	598	1.14
NM-03	3.54	2.30	4.2	0.130	223	0.67	595	0.87
ZM510	4.01	3.17	7.9	0.121	226	0.85	622	1.05
ZM760	1.08	0.77	2.7	0.089	199	0.18	570	0.32
ZM950	0.52	0.43	4.0	0.059	195	0.09	554	0.12
S1-Na	6.50	6.50	0.0	0.129	—	—	—	—
S1-H	6.73	6.53	13.1	0.122	236	0.99	626	2.20
S1-1 *N*	6.42	5.88	17.4	0.130	229	1.08	578	2.07
S1-6 *N*	6.45	5.44	15.2	0.142	228	0.87	600	2.15
S1-01	6.08	3.89	4.8	0.143	236	1.03	601	1.17
S1-02	0.92	0.85	3.2	0.115	—	—	—	—
S1-03	0.87	0.85	2.7	0.104	203	0.28	591	0.37
S1-02II	0.91	0.89	3.4	0.095	205	0.28	595	0.35
S1-03II	0.87	0.86	2.9	0.075	205	0.27	591	0.29
S2-Na	6.41	6.41	0.0	0.116	—	—	—	—
S2-H	6.70	5.89	13.3	0.118	227	0.63	600	1.66
S2-1 *N*	6.12	5.42	19.8	0.116	226	0.71	559	1.54
S2-6 *N*	6.09	5.21	16.6	0.110	228	0.62	580	1.52
S2-01	6.40	4.96	13.0	0.132	223	0.57	587	1.70
S2-02	4.17	3.21	7.8	0.140	234	0.69	606	0.95
S2-03	2.77	2.33	9.3	0.125	215	0.48	590	0.58

to 65% for NM-03. The octahedral resonance of NM-01 was very broad but narrowed considerably for the refluxed samples (Table 2). The ZM samples contained between 72 and 82% of their aluminum in the tetrahedral form. The octahedral resonance of ZM510 was relatively broad whereas this peak for ZM760 and ZM980 was much sharper. The sodium forms of S1 and S2 contained no octahedral aluminum. After both reflux procedures, the percentage aluminum exhibiting tetrahedral coordination in the S1 mordenite had increased from 64% for S1-01 to 98% for S1-03, whereas in the case of S2-03 this was only 84%. The octahedral resonances of the acid-treated S1 samples were quite narrow, especially those of the refluxed samples, while those of the acid-treated S2 samples were broader.

Catalyst Acidity

The ammonia TPD spectra exhibited two characteristic peaks, a low-temperature desorption (LTD) peak between 195 and 244°C and a high-temperature desorption (HTD) peak between 554 and 626°C. The LTD peak is a result of physisorbed NH_3 and NH_3 which has not been flushed from the zeolite pores prior to initiation of the temperature ramp. The size and maximum temperature of this peak are not indicative of the acidic nature of the catalyst. The HTD peak is related to the strong acidity resulting from aluminum in the zeolite framework (*24, 25*). The peak temperatures and desorption concentrations are listed in Table 2. Figure 2 shows the existence of a linear relationship between the number of tetrahedral aluminum species generating acid sites (not tetrahedral aluminum species charged balanced

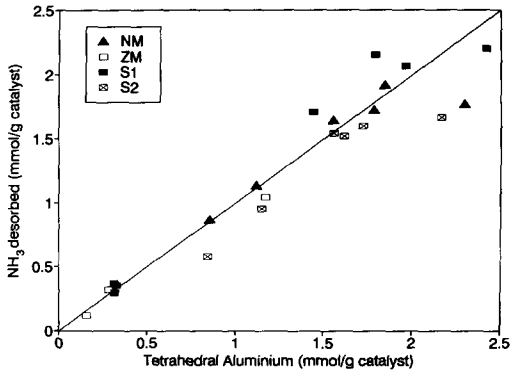

FIG. 2. HTD NH_3 as a function of tetrahedral aluminum species generating acid sites.

by Na^+ ions) and the amount of ammonia desorbing from these sites (HTD peak) for acid-dealuminated samples.

The temperatures of both HTD and LTD peaks decreased with decreasing tetrahedral aluminum content. The extent to which the HTD peak temperature decreased was not the same for the different mordenite samples. The ZM samples showed a large decrease in peak temperature, going from 622 to 554°C as the framework aluminum content decreased from 3.17 to 0.43 wt%. This was not the case for the NM, S1, or S2 samples where the peak temperature decreased only from 626 to 591°C as the aluminum content decreased from 6.53 to 0.85 wt%.

Infrared Spectroscopy

Infrared spectra of the catalyst samples showed that the ν_{as} T-O band shifted from 1060 to 1089 cm^{-1} as the extent of dealumination increased (Table 1). The spectra of the ZM samples differed from those of the other mordenites in that the structural bands (400–900 cm^{-1}) were clearly resolved, their resolution increasing as the amount of aluminum in these samples decreased.

The 955 cm^{-1} shoulder observed by Dunken and Stephanowitz and Musa *et al.* (*18*) was not seen in the spectra of any of the ZM samples. This band was not evident in the spectra of the sodium mordenites but did appear as a slight shoulder in the spectra of the ammonium-exchanged NM, S1, and S2 samples. The intensity of this shoulder increased as the framework aluminum content decreased (Fig. 3). As can be seen in Fig. 4, there is a direct relationship between the area under the 955 cm^{-1} shoulder of the NM, S1, and S2 samples and the amount of aluminum removed from the mordenite framework. Calcination of the S1-02 sample at 650 and 800°C resulted in no significant reduction of the 955 cm^{-1} shoulder and very little shift in any of the band positions.

The peak at 800 cm^{-1} did not increase on dealumination of the mordenite samples but shifted to slightly higher wavenumbers and became more clearly resolved as the intensity of the 710–750 cm^{-1} band decreased (Fig. 3). This 800–820 cm^{-1} band was particularly sharp for the ZM samples (Fig. 5) becoming sharper as the extent of dealumination increased.

The 620–630 cm^{-1} band and the broadband between 710 and 750 cm^{-1} were seen in all the nondealuminated samples. On dealumination, the 620–630 cm^{-1} band shifted to higher wavenumbers but was not signifi-

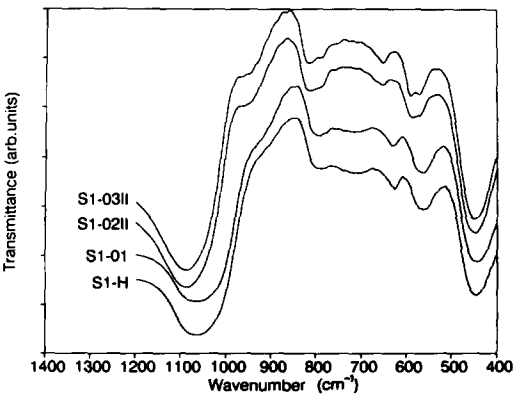

FIG. 3. Effect of acid dealumination on the infrared spectra of S1 mordenite.

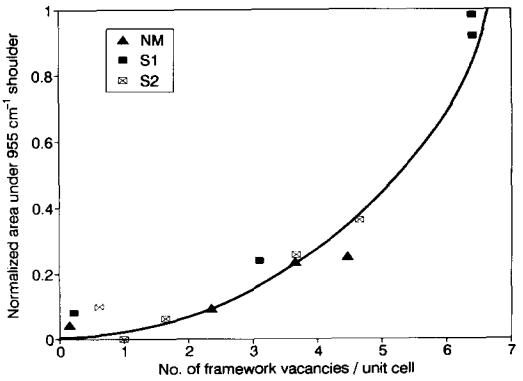

FIG. 4. Normalized area under the 955 cm^{-1} shoulder as a function of the number of framework vacancies (per unit cell) produced as a result of aluminum extraction.

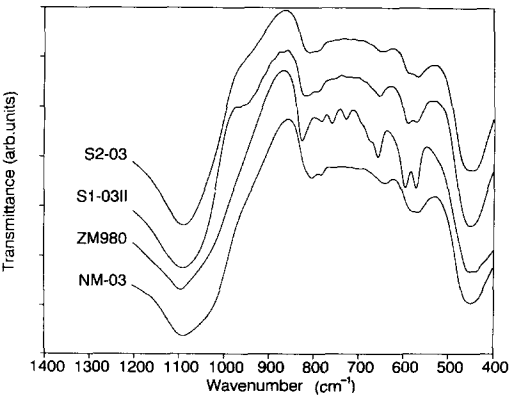

FIG. 5. Infrared spectra of the most severely dealuminated forms of the NM, ZM, S1, and S2 mordenites.

cantly reduced, whereas the 710–750 cm^{-1} band decreased as the aluminum content of the catalyst samples decreased (Fig. 3).

Cyclohexane Adsorption and Surface Areas

The cyclohexane adsorption levels decreased as the aluminum content of the catalyst decreased as a result of dealumination (Table 1). There are clear differences between the cyclohexane adsorption profiles of the NM, S1, and S2 mordenites, the S1 mordenite adsorbing more cyclohexane than the NM and S2 mordenites for equivalent tetrahedral aluminum contents (Fig. 6). It is also clear that the cyclohexane adsorption levels of the mordenites increase on initial dealumination. The cyclohexane adsorption levels of the S1 samples dropped from 10.2 wt% for S1-6*N* to 5.1 wt% for S1-02. The severely acid-treated sample S1-03 II adsorbed only 3.5 wt% cyclohexane although the aluminum content of this catalyst was only slightly less than that of S1-02 II.

The surface areas of all the samples were greater than 350 m^2/g. The surface areas of the mildly acid-treated samples generally decreased from that of the H form but increased with progressive acid refluxing (Table 1). In all the cases the -03 samples exhibited greater surface areas than the H forms.

DISCUSSION

Catalyst Dealumination

The increasing extent of framework dealumination with successive leaching cycles of the S1 mordenite compared with that of the NM and S2 materials (Table 1) can be ascribed to the differences in crystallite sizes of these materials. The smaller S1 crystallites present less intracrystalline diffusional restrictions to the leaching process than do the larger crystallites of the NM and S2 materials. These diffusional restrictions

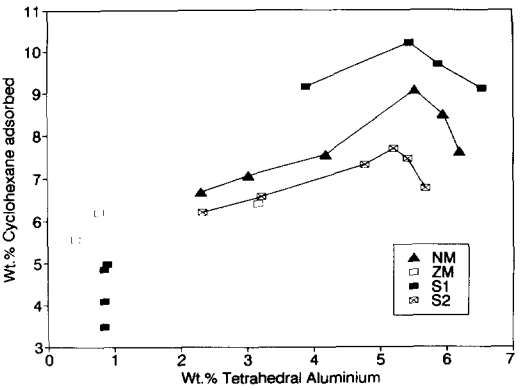

FIG. 6. Cyclohexane adsorbed as a function of tetrahedral aluminum content (of the dry catalyst).

would be increased by the presence of extraframework silicon species deposited during the catalyst synthesis. The differing dealumination rates cannot be ascribed to varying amounts of 2-D channel structure material (*Cmmm* point group—lower diffusional resistance) and the more common 1-D channel structure material (*Cmcm* point group—higher diffusional resistance) as described by Musa *et al.* (*18*). XRD spectra show no evidence for the presence of the *Cmmm* space group variant (absence of a reflection of $2\theta = 15.31°$) nor is the appearance of significant amounts of amorphous material (resulting from the decomposition of the less thermally stable *Cmmm* material (*18*)) seen in any of the electron micrographs. The amount of tetrahedral aluminum remaining in the S1-02 and S1-03 samples was approximately one-eighth of the aluminum initially present. There are approximately eight aluminum atoms per unit cell in unmodified mordenite and thus, under the leach conditions used, one aluminum atom appears to be more stably bound in the crystal structure.

This effect of crystallite size is not expected to be limited to the extent of framework dealumination, but should also influence the extent of removal of the resulting extraframework aluminum species from the crystallites. Thus, the significantly higher octahedral content of the NM and S2 samples, versus that of the S1 material, can also be explained by the smaller S1 crystallites from which the extraframework aluminum species can diffuse more easily. Furthermore, the relative sharpness of the S1 and ZM octahedral aluminum resonances indicate these octahedral species to be highly mobile, hydrated, and located in the main 12-ring channels (*14*). In contrast, the broad resonances observed for the refluxed NM and S2 samples suggest that a large fraction of the octahedral aluminum species located in these materials is located in the 8-ring side channels.

A sequence of dealumination events is proposed in which framework dealumination takes place simultaneously in the main channels and the side pockets. Extraframework aluminum species in the main channels are hydrated oxyhydroxy species which readily diffuse out of the crystallite into the bulk leaching medium. Extraframework aluminum species within the side pockets are partially hydrated (*14*). As the main channel species diffuse out of the crystallites, the side pocket extraframework species migrate into the main channels where they become fully hydrated and, in turn, diffuse out of the crystallites.

Catalyst Acidity

The NH_3 desorption temperatures, especially those of the HTD peaks, are higher than those previously reported (*22, 25–27*). This is due to NH_3 readsorption which was caused by the low carrier/sample ratio employed for the purpose of increasing the NH_3 concentration levels in the thermal conductivity detector.

On dealumination the number of acid sites available for NH_3 readsorption decreases and the reduced readsorption results in a lower peak maximum temperature. Thus, the results of this study, viz. the decrease in the HTD peak maximum temperature with increasing dealumination, do not necessarily imply a decrease in the acid site strength as dealumination proceeds. Indeed, other workers (*28*) using a vacuum TPD system in which the influence of readsorption is negligible observed an increase in the strength of strong Brønsted acid sites with increasing severity of dealumination.

Regardless of the difficulties introduced due to NH_3 readsorption in this study, the total acidity of the samples as measured by the total HTD NH_3 is still correctly determined by these measurements. There is a good 1 : 1 relationship between the amount of HTD NH_3 and the tetrahedral aluminum content of all the -01, -02, and -03 samples. As the -1 *N* and -6 *N* samples still contained significant amounts of sodium, the tetrahedral aluminum contents plotted in Fig. 2 reflect aluminum species generating acid sites and not aluminum species which are charge

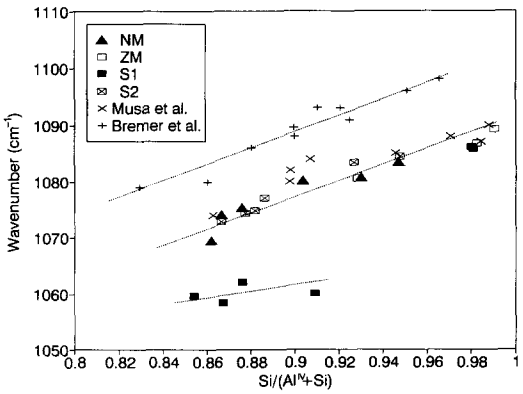

FIG. 7. Shift in the position of the T–O stretching band as a function of the $Si/(Al^{IV} + Si)$ ratio.

balanced by Na^+ ions. The slight reduction in the amount of HTD NH_3 for the -H samples is ascribed to reduced accessibility of framework aluminum due to the presence of nonstructural species deposited on the crystallite surface or in the channel structure during synthesis. The reduced accessibility of the zeolite channels of the -H samples is also seen in the cyclohexane adsorption levels of these samples indicating that acid treatment facilitates the removal of these species resulting in a more accessible pore volume, as was also reported by Chen (*29*).

Sawa *et al.* (*22*) found that, for mordenites with aluminum contents of greater than 1.65 mmol/g, the amount of HTD NH_3 decreased with framework aluminum content. As the only samples in their work for which the HTD NH_3/framework aluminum ratio was found to decrease were unmodified, it is suggested that the accessibility to aluminum in these samples may have been similarly restricted due to the presence of nonstructural species in the zeolite channels.

Structural Characterization

The shift in the ν_{as} T-O band with reduction in aluminum content has been reported by other workers (*18, 30*) and their data are compared with those obtained in this study in Fig. 7. The results of this study are similar to those reported by Musa *et al.* (*18*) in which the band frequency is observed to shift in the range 1060–1090 cm^{-1} as dealumination proceeds to completion. The trend of the ν_{as} T-O band as a function of tetrahedral aluminum content of the mildly dealuminated S1 samples lies below that of the other mordenites. The data presented by Bremer *et al.* (*30*) indicate that the Si/Al + Si ratio of mordenites may be monitored by the shift in the position of the ν_{as} T-O band. From the results obtained in this study as well as those obtained by Musa *et al.*, it would appear that infrared spectroscopy is an unreliable method for monitoring this Si(Al + Si) ratio.

Several workers (*16–18*) have postulated that, when dealumination occurs without silicon substituting for extracted aluminum, new $O_3Si–O–SiO_3$ bonds may be formed between SiO_4 tetrahedra previously linked via AlO_4 tetrahedra. Ha *et al.* (*20*) previously attributed an increase in the 820 cm^{-1} band to the formation of these new $O_3Si–O–SiO_3$ bonds. In the present study, however, no relationship was found between the magnitude of the 820 cm^{-1} band and the amount of framework aluminum removed.

Beyer *et al.* (*15*) attributed the 955 cm^{-1} peak to the presence of hydroxyl nests formed on the removal of aluminum from the zeolite framework. Fejes *et al.* (*31*) suggested that such hydroxyl nests would have a low thermal stability and should decompose at low temperatures. As no reduction in the 955 cm^{-1} band was seen in the spectra of the S1-02 II samples calcined at 650 and 800°C, it seems unlikely that such nests can be associated with the 955 cm^{-1} band. The inability to incorporate silicon into such nests (*32*) is further evidence against the presence of these nests in calcined samples.

From the results of this study it can be seen that the 955 cm^{-1} band was the only structural infrared band which increased in intensity as the number of T vacancies resulting from aluminum extraction in the mordenite structure increased (Fig. 5). The above findings confirm that the 955 cm^{-1}

band, noticeably present in the acid-treated S1 and S2 samples, results from the formation of new $O_3Si–O–SiO_3$ bonds. These bonds would be longer than the normal T-O bonds since they stretch across vacancies formed by the extracted aluminum and hence the appearance of this new band at lower frequencies than that of the undistorted T-O bonds.

The infrared spectra of the ZM samples exhibit no band at 955 cm^{-1}. This is to be expected since the dealumination procedure employed for these samples is conducive for the replacement of extracted aluminum by silicon (*33*) and, consequently, new $O_3Si–O–SiO_3$ bonds responsible for the 955 cm^{-1} band are not formed. The various structural bands and the ν_{as} T-O band are, however, narrower than those of the NM, S1, and S2 samples as would be expected since silicon has replaced aluminum (which has a longer bond length with oxygen) and thus the average variation in the T-O bond length of the ZM samples is less.

Given this assignment of the 955 cm^{-1} band to new $O_3Si–O–SiO_3$ bonds formed upon dealumination, it is likely that the assignment of the 820 cm^{-1} band to external symmetric stretching vibrations is correct (*19, 34*). The results shown in Fig. 3 show the frequency of this vibration to shift from 800 to 818 cm^{-1} as dealumination approaches completion, in the same manner that the asymmetric stretching vibration shifts from 1060 to 1086 cm^{-1}.

As found by other workers (*18, 35*), the intensity of the broadband in the region 710–750 cm^{-1} decreased with decreasing framework aluminum content (Fig. 3). This result is consistent with the previously reported association of a band at 720 cm^{-1} to framework aluminum in mordenite (20, 35).

Upon dealumination, the band in the 620–630 cm^{-1} region is observed to shift to higher wavenumbers without any accompanying loss in intensity (Fig. 3). This band is also present at similar intensities in the highly dealuminated ZM980 sample (Fig. 5). The assignment of this band to isolated AlO_4 tetrahedra (*13*) or alternating SiO_4 and AlO_4 tetrahedra (*20*) is therefore not supported by these results and it is more likely that the correct assignment is that proposed by Coudurier *et al.* (*36*) to single 4-ring vibrations. The shift in this band upon dealumination is, therefore, analogous to the shifts in the 1060–1090 and 800–818 cm^{-1} regions as described above.

For the acid-leached samples (NM, S1, S2) the unit cell parameters and the relative crystallinities are generally observed to decrease with decreasing aluminum content. In contrast, the unit cell parameters of the ZM samples are essentially identical, irrespective of aluminum content, and the relative crystallinity was observed to increase with decreasing aluminum content (Table 1). These results are in accordance with expected trends given the removal of aluminum T atoms in the acid-leached samples and their replacement by silicon in the ZM samples. Extraction of aluminum results in a reduced unit cell size and a distorted framework structure brought about by the new bonds between $SiO_{4/2}$ tetrahedra previously linked to $AlO_{4/2}$ tetrahedra. Replacement of lost aluminum by silicon results in an increasingly crystalline framework structure formed when $SiO_{4/2}$ tetrahedra replace $AlO_{4/2}$ tetrahedra and the deviation in the T-O bond lengths becomes less.

Cyclohexane Adsorption and Surface Areas

Cyclohexane adsorption levels (Table 1) indicate that all unmodified catalyst samples were large-port mordenite since the adsorption levels of small-port mordenites are about 1% (*12*). Upon initial dealumination, the quantity of cyclohexane adsorbed increased from that of the -H and -Na form samples. This trend was also found by Chen (*29*) who ascribed this initial increase in cyclohexane adsorption levels to the removal of extraneous materials from the mordenite channels. The cyclohexane adsorption levels of the more severely dealuminated samples decreased and it is likely that this

decrease is due to the simultaneous progressive decrease in channel diameter, thereby limiting the capacity for cyclohexane adsorption. That such a decrease in channel diameter occurs with dealumination may be deduced from the observed reduction in unit cell parameters (Table 1). In contrast to the NM, S1, and S2 materials, the cyclohexane adsorption capacities of the ZM samples are essentially constant with decreasing aluminum content as are their unit cell parameters. This result is consistent with the dealumination procedure employed for the ZM catalysts in which the extracted aluminum is replaced by silicon, thereby stabilizing the zeolite framework. The initial increase in cyclohexane adsorption capacity from that of the -H and -Na forms is ascribed to the removal of acid-soluble nonstructural species desposited in the channels or on the crystallite surface during synthesis. It is likely that the nonstructural species are silicon based as there is very little extraframework aluminum in the channels of the S1-H and S2-H samples as indicated by ^{27}Al MAS NMR. Furthermore, all organic material is removed by combustion during calcination.

The surface areas of the acid-leached samples decreased after initial dealumination (samples designated -01) but increased with further dealumination. These results are consistent with the sequence of dealumination steps proposed above in that the initial decrease in surface area is most likely due to partial blocking of the side pockets. Further dealumination and subsequent removal of leached aluminum species from the side pockets would result in the observed increase in surface area. The surface areas of the severely dealuminated samples exceeded those of the H form of the catalyst. This suggests that severe dealumination may result in the linking of side pockets of adjacent main channels as described by Barrer and Petersen (*37*). Such a linking of side pockets provides both additional virgin surface area and possible accessibility to previously inaccessible channel volume. For the severely dealuminated samples, cyclohexane adsorption levels are low while the BET surface areas exceed those of the starting materials. These results are to be expected as the side pockets are accessible to nitrogen but not cyclohexane.

CONCLUSIONS

The findings of this study show that mordenite materials may dealuminate quite differently even though they exhibit the characteristic mordenite XRD reflections. The extent of dealumination is strongly influenced by the mordenite crystallite size, with smaller crystallite size materials dealuminating most rapidly. Dealumination progresses rapidly to an aluminum content of approximately one aluminum per unit cell, suggesting that this last aluminum is stably bound in the crystal structure and may require severe dealumination conditions for its removal. Extensively dealuminated samples retain their characteristic mordenite structure and exhibit larger surface areas than their parent materials.

For acid-dealuminated mordenites, NH_3 TPD (HTD peak) may be used to determine framework aluminum content, irrespective of the presence of extraframework aluminum. Infrared spectroscopy, on the other hand, is not a reliable tool for determining the tetrahedral aluminum content of mordenites. In agreement with other authors, the 955 cm^{-1} infrared band is assigned to vibrations from new $O_3Si–O–SiO_3$ bonds formed upon framework aluminum extraction during the dealumination process.

Consistent with the findings of this study, it is proposed that nitric acid dealumination of mordenites takes place in accordance with the following process: (i) Framework dealumination occurs simultaneously in the main channels and the side pockets; (ii) extraframework aluminum species in the main channels are hydrated oxyhydroxy species which readily diffuse out of the crystallite into the bulk leaching medium; and (iii) as the main channel species diffuse out of the crystallites, partially hydrated extraframework species within the side pockets mi-

grate into the main channels where they become fully hydrated and, in turn, diffuse out of the crystallites.

ACKNOWLEDGMENTS

The authors acknowledge financial support from the Foundation for Research and Development, AECI, and the University of Cape Town. The invaluable contribution of Dr. M. Kojima is also gratefully acknowledged.

REFERENCES

1. Giordano, W., Vitarelli, P., Cavallaro, S., Otanna, R., and Lembo, R., *in* "Proceedings, 6th International Zeolite Conference" (D. Olson and A. Bisio, Eds.), p. 331. Butterworths, London, 1984.
2. Bandiera, J., Hamon, C., and Naccache, C., *in* "Proceedings, 6th International Zeolite Conference" (D. Olson and A. Bisio, Eds.), p. 337. Butterworths, London, 1984.
3. Pardillos, J., Coq, B., and Figueras, F., *Appl. Catal.* **51,** 285 (1989).
4. Niwa, M., Sawa, M., and Murakami, Y., *in* "Proceedings, 9th International Congress on Catalysis, Calgary, 1988" (M. J. Phillips and M. Ternan, Eds.), p. 380. Chem. Institute of Canada, Ottawa, 1988.
5. De Armando, M., Gnep, N., and Guisnet, M., *J. Chem. Res.* **1,** 8 (1981).
6. Scherzer, J., "Catalytic Materials: Relationship between Structure and Reactivity" (T. E. Whyte *et al.*, Eds.), Am. Chem. Soc. Symp. Ser., Vol. 248, p. 157. Am. Chem. Soc., Washington, DC, 1984.
7. Karge, H. G. and Weitkamp, J., *Chem. Ing. Technol.***58,** 946 (1986).
8. Bhavikatti, S. S., and Patwardhan, S. R., *Ind. Eng. Chem. Prod. Res. Dev.* **20,** 102 (1981).
9. Koradia, P. B., Kiovsky, J. R., and Asim, M. Y., *J. Catal.* **66,** 290 (1980).
10. Haas, J., Fetting, F., and Gubicza, L., *Acta Phys. Chem.* **31,** 659 (1985).
11. Itabashi, K., Fukushima, T., and Igawa, K., *Zeolites* **6,** 30 (1986).
12. Raatz, F., Freund, E., and Marcilly, C., *J. Chem. Soc. Faraday Trans. 1* **79,** 2299 (1983).
13. Van Geem, P. C., Scholle, K. F. M., van der Velden, G. P. M., and Veeman, W. S., *J. Phys. Chem.* **92,** 1585 (1988).
14. Goovaerts, F., Vansant, E. F., Pilippaerts, J., De Hulsters, P., and Gelan, J., *J. Chem. Soc. Faraday Trans. 1* **85,** 3675 (1989).
15. Beyer, H. K., Belanykaja, I. M., Mishin, I. V., and Borbely, G., *in* "Proceedings, Conf. Structure and Reactivity of Modified Zeolites" (P. A. Jacobs, N. I. Jaeger, P. Jiru, G. Schulzekloff, and V. B. Kazansky, Eds.), p. 1233. Elsevier, Amsterdam, 1984.
16. Fejes, P., Hannus, I., and Kiricsi, I., *Zeolites* **4,** 73 (1984).
17. Dunken, H., and Stephanowitz, R., *Z. Chem.* **23,** 353 (1983).
18. Musa, M., Tarina, V., Stoica, A. D., Ivanov, E., Postinaru, D., Pop, E., Pop, Gr., Ganea, R., Birjega, R., Musca, G., and Paukshtis, E. A., *Zeolites* **7,** 427 (1987).
19. Flanigen, E. M., *in* "Zeolite Chemistry and Catalysis" (J. A. Rabo, Ed.), Am. Chem. Soc. Monograph Ser., Vol. 171, Chap. 2. Am. Chem. Soc., Washington, DC, 1976.
20. Ha, B., Guidot, J., and Barthomeuf, D., *J. Chem. Soc. Faraday Trans. 1* **75,** 1245 (1979).
21. Karge, H. G., Wada, Y., Weitkamp, J., Ernst, S., Girrbach, U., and Beyer, H. K., *in* "Catalysis on the Energy Scene" (S. Kaliaguine and A. Mahay, Eds.), p. 101. Elsevier, Amsterdam, 1984.
22. Sawa, M., Niwa, M., and Murakami, Y., *Zeolites* **10,** 532 (1990).
23. Fernandez, C., Lefebvre, F., Nagya, J. B., and Derouane, E. G., *in* "Innovation in Zeolite Materials Science" (P. J. Grobet *et al.*, Eds.), p. 223. Elsevier, Amsterdam, 1988.
24. Sawa, M., Niwa, M., and Murakami, Y., *Appl. Catal.* **53,** 169 (1989).
25. Meyers, B. L., Fleisch, T. H., Ray, J. T. Miller, G. J., and Hall, J. B., *J. Catal.* **110,** 84 (1988).
26. Hidalgo, C. V., Itoh, H., Hattori, T., Niwa, M., and Murakami, Y., *J. Catal.* **85,** 362 (1984).
27. Miradatos, C., Ha, B. H., Otsuka, K., and Barthomeuf, D., *in* "Proceedings, 5th International Zeolite Conference" (L. Rees, Ed.), p. 382. Heyden, London, 1980.
28. Karge, H. G., and Dondur, V., *J. Phys. Chem.* **94,** 765 (1990).
29. Chen, N. Y., *J. Phys. Chem.* **80,** 60 (1976).
30. Bremer, H., Reschetilowski, W., Ahmed, A. S., Wendlant, K. P., Nau, P. E., and Mishin, I. V., *Z. Chem.* **23,** 381 (1983).
31. Fejes, P., Hannus, I., Kiricsi, I., Pfeifer, H., Freude, D., and Oehme, W., *Zeolites* **5,** 45 (1985).
32. Barrer, R.M., *in*"Zeolites and Clay Minerals as Sorbents and Molecular Sieves," p. 358. Academic Press, London, 1978.
33. Jacobs, P. A., "Carboniogenic Activity of Zeolites," p. 52. Elsevier, Amsterdam, 1977.
34. Breck, D. W., "Zeolite Molecular Sieves," p. 418. Wiley, New York, 1974.
35. Pichat, P., Beaumont, R., and Barthomeuf, D., *J. Chem. Soc. Faraday Trans. 1* **70,** 1402 (1974).
36. Coudurier, G., Naccache, C., and Vedrine, J. C., *J. Chem. Soc. Chem. Commun.* **24,** 1413 (1982).
37. Barrer, R. M., and Peterson, D. L., *Proc. R. Soc. London A* **280,** 468 (1964).